



C: Surfaces, Interfaces, Porous Materials, and Catalysis

Decoupling Catalyst Dewetting, Gas Decomposition, and Surface Reactions in Carbon Nanotube Forest Growth Reveals Dependence of Density on Nucleation Temperature

Jaegeun Lee, Moataz Abdulhafez, and Mostafa Bedewy

J. Phys. Chem. C, Just Accepted Manuscript • DOI: 10.1021/acs.jpcc.9b07894 • Publication Date (Web): 05 Nov 2019

Downloaded from pubs.acs.org on November 8, 2019

Just Accepted

"Just Accepted" manuscripts have been peer-reviewed and accepted for publication. They are posted online prior to technical editing, formatting for publication and author proofing. The American Chemical Society provides "Just Accepted" as a service to the research community to expedite the dissemination of scientific material as soon as possible after acceptance. "Just Accepted" manuscripts appear in full in PDF format accompanied by an HTML abstract. "Just Accepted" manuscripts have been fully peer reviewed, but should not be considered the official version of record. They are citable by the Digital Object Identifier (DOI®). "Just Accepted" is an optional service offered to authors. Therefore, the "Just Accepted" Web site may not include all articles that will be published in the journal. After a manuscript is technically edited and formatted, it will be removed from the "Just Accepted" Web site and published as an ASAP article. Note that technical editing may introduce minor changes to the manuscript text and/or graphics which could affect content, and all legal disclaimers and ethical guidelines that apply to the journal pertain. ACS cannot be held responsible for errors or consequences arising from the use of information contained in these "Just Accepted" manuscripts.

Decoupling Catalyst Dewetting, Gas Decomposition, and Surface Reactions in Carbon Nanotube Forest Growth Reveals Dependence of Density on Nucleation Temperature

Jaegeun Lee^{1,2†}, Moataz Abdulhafez^{1†}, and Mostafa Bedewy^{1,3,4*}

¹Department of Industrial Engineering, University of Pittsburgh, 3700 O'Hara Street, Pittsburgh, PA 15261, USA

²Current address: Department of Organic Material Science and Engineering, Pusan National University, 2, Busandaehak-ro 63 beon-gil, Geumjeong-gu, Busan, 46241, Republic of Korea

³Department of Chemical and Petroleum Engineering, University of Pittsburgh, 3700 O'Hara Street, Pittsburgh, PA 15261, USA

⁴Department of Mechanical Engineering and Materials Science, University of Pittsburgh, 3700 O'Hara Street, Pittsburgh, PA 15261, USA

E-mail address: mbedewy@pitt.edu (M. Bedewy)

[†]These authors contributed equally to this work.

^{*}author to whom correspondence should be addressed.

Abstract

In chemical vapor deposition (CVD) of vertically aligned carbon nanotubes (CNTs), temperatures for the following three processes are typically coupled: (1) catalyst nanoparticle formation by film dewetting, (2) thermal decomposition of gas precursors, and (3) nucleation/growth of CNTs. Here, we present an approach for complete decoupling of these processes using a custom-designed multizone rapid thermal CVD reactor. We show that in decoupled growth, there is an inverse relationship between density of CNTs and nucleation temperature, while there is no dependence of density on catalyst formation temperature. Importantly, the nucleation/growth temperature that produces the most aligned and densest CNTs is lower than the temperature that produces the tallest CNTs. We also reveal that this inverse relation of density is not because of decreased number density of catalyst nanoparticles, but is rather caused by a marked decrease in the percentage of active catalyst at high nucleation temperatures. A mechanism is proposed to explain this phenomenon based on local spatial nonuniformities of carbon supply in the vicinity of fastgrowing CNTs, causing starvation at neighboring catalyst manifested as lower percentage of activation at high temperatures. Our results provide insights into the fundamental tradeoff between requirements for higher CNT density/alignment, and taller CNT structures.

1. INTRODUCTION

Individual carbon nanotubes (CNTs) are interesting building blocks in many nanotechnology applications, because they possess excellent mechanical, thermal, and electrical properties. CNT forests, in which CNTs grow vertically aligned on a substrate, combines the excellent properties of individual CNTs with unique anisotropy of collective properties arising from their high degree of alignment and high density. Since a CNT forest is a population of billions (or sometimes trillions) of CNTs/cm², its collective properties are largely influenced by how individual CNTs interact with each other and self-organize during growth (i.e., spatiotemporal evolution of alignment and areal number density during growth), in addition to the intrinsic properties of the individual CNTs such as diameter, number of walls, and chirality. In particular, controlling the areal number density of CNTs is required for the successful applications of CNT forests as electrical interconnects in integrated circuits.^{5,6} thermal interfaces in high power density electtronics.⁷ and flow membranes in separation and purification applications. For example, in the case of integrated circuits, to replace copper interconnects, the required areal number density of CNTs needs to be at least 2 × 10¹³/cm² to outperform copper, ⁵ which is still challenging especially for as-grown CNT forests without post-growth densification.

Despite its importance, however, the growth of density-controlled CNT forests from catalyst nanoparticles by catalytic chemical vapor deposition (CVD) using gaseous carbon precursor is still not well understood.^{9–13} Generally, it has been found that the areal number density of CNTs has a positive correlation with that of catalyst nanoparticles.^{5,6,14} Importantly, it has been frequently reported that not all of the catalyst nanoparticles on the substrate can be activated to nucleate CNTs, ^{15–17} and it remains unclear how to control the proportion of activated catalysts, referred to

as the activation percentage or CNT nucleation success fraction.

The main challenge lies in the complexity of the multistep chemical and physical processes involved in CNT forest growth. Typically, the growth of a CNT forest by catalytic CVD consists of three distinct processes that are often coupled: (1) the formation of catalyst nanoparticles by thin film dewetting, (2) the decomposition of gas-phase carbon precursors, and (3) the nucleation and growth of CNTs on the catalytic surfaces of nanoparticles. Typically, the thin-film catalyst, 1 nm Fe in our case, is first reduced and transformed into a population of nanoparticles by means of solid state dewetting upon heating in a reducing environment. 18–20 To start the growth process, a carbon precursor is introduced in the CVD reactor in the gas phase, which undergoes thermal decomposition in the gas phase (if the temperature is high enough) before reaching the surface of the catalyst nanoparticles. Some of the thermal decomposition products are active species that take part in incorporating carbon atoms into an ordered cap that then lifts-off as a CNT growing from a catalyst nanoparticle. 21,22 In typical CVD growth systems, such as hot-walled tube furnaces, the temperatures for these processes are inevitably coupled; the temperature at which gas-phase decomposition occurs and the temperature at which catalyst nanoparticles are formed are roughly similar to, or dependent on, the temperature of catalytic growth of CNTs. As a result of the coupled nature of growth explained above, we are currently limited in our ability to comprehensively understand and accurately control the entire growth processes. In particular, this coupled growth is hindering the independent investigation of conditions governing CNT nucleation and activation percentage in a large population separately from both the conditions governing the catalyst preparation and the gas decomposition steps.

Hence, "decoupling" of these processes is sought after, and there have been efforts by several

groups towards decoupling, as summarized in Table 1. To decouple the gas-phase decomposition from the catalytic growth of CNTs, one approach adopted previously was based on using a separate preheater wherein decomposition of gas-phase precursor occurs.^{21–24} Also, tungsten wire filament was used to accelerate the gas-phase reactions.²⁵ Another approach based on creating a vertical temperature gradient inside the CVD reactor was utilized, where the temperature profile of the gas phase was controlled by two heaters, one above and the other below the substrate.^{26,27} Compared to the efforts to decouple gas-phase decomposition from CNT nucleation and growth, there is much less work on decoupling of catalyst formation from the catalytic growth of CNTs. One approach to achieve this was based on rapid thermal processing,^{28,29} while another approach was based on moving the substrate rapidly in and out of the CVD reactor using a transfer arm.³⁰ However, there is no report on decoupling both gas-phase reaction and catalyst formation from the CNT growth at the same time. This may be due the complexity of reactor design that such complete decoupling entails.

Here, we present an approach, as shown in Fig. 1, for complete decoupling of the catalyst formation temperature (T_c), the gas-phase decomposition temperature (T_p), and the CNT nucleation and growth temperature (T_g). This is achieved based on our unique custom-designed multizone rapid thermal CVD reactor. Our decoupling approach enables unprecedented independent investigation of the effect of each of the three temperatures (T_p , T_c , and T_g) on the as-grown CNT forest. Accordingly, we demonstrate that areal number density of CNTs is dependent on nucleation temperature (T_g), while being largely independent on catalyst formation temperature (T_c).

2. EXPERIMENTAL METHODS

2.1. CNT forest growth

Experimental information is summarized in Fig. 2. CNTs were grown in a custom-designed multizone rapid thermal CVD reactor (CVD Equipment, Central Islip, NY) (Fig. 2a). As a substrate, silicon (100) wafer with a 300-nm thick SiO₂ layer was used. A 10 nm-thick alumina layer was deposited by atomic layer deposition and a 1 nm-thick Fe layer was deposited by e-beam evaporation.³³ For each growth, the substrate was cut into small pieces of 5 mm × 5 mm. Before every growth, the reactor was air-baked at 1000 °C for 25 min to remove carbonaceous contaminants on the reactor wall. Then, a piece of catalyst-coated substrate was loaded into the reactor and a growth was run automatically according to a programmed recipe. Every recipe includes a vacuum-baking step before the catalyst formation step to ensure consistent growth result by effectively removing oxygen-containing impurities on and in the reactor wall.³¹ A growth recipe is shown in Fig. 2c, in which the total flow rate was 1700 sccm. During the catalyst formation step, the flow rates of He, He through the water bubbler, and H₂ were 1010, 200, and 490 sccm, respectively. During the growth step, the flow rates of He, He through the water bubbler, H₂, and C₂H₄ were 640, 200, 490, and 370 sccm, respectively. The concentration of water vapor carried by 200 sccm of He through the water bubbler is calculated to be approximately 116 ppm.

2.2. Measuring forest height and density

A 3D optical microscope (VR-3000 series, Keyence) was used for accurate measurements of forest height and volume. Using the 3D optical microscope, we measured the volume of a CNT forest

(Fig. 2b). The height of a CNT forest was obtained by dividing the volume of a CNT forest by the area of the substrate. The volumetric mass density of a CNT forest was obtained by dividing the mass of a CNT forest by its volume.

2.3. Characterization of morphology and quality of CNTs

The morphology of the as-grown CNT forests was analyzed by scanning electron microscopy (SEM) using JEOL JSM-6510. The structural quality was assessed by Raman spectroscopy (Xplora, Horiba Scientific) using the 638 nm excitation wavelength. The outer diameter and number of walls of CNTs were characterized by transmission electron microscopy (TEM) using Hitachi H9500.

2.4. Characterization of catalyst nanoparticles

The size distribution and number density of catalyst nanoparticles were characterized by atomic force microscopy (AFM) using Veeco Dimension 3100 V. As a measure of the size of nanoparticles, we used height of nanoparticles. The nanoparticles were detected by the watershed algorithm provided by Gwyddion software (http://gwyddion.net/). The detailed parameters we used in the algorithm are as follow: for grain location, number of steps: 10, drop size: 10%, and threshold: 3 px 2 and for segmentation, number of steps: 10, drop size: 40%. We used z_{max} of each grain as the height of each particle.

2.5. Quantification of CNT alignment

We analyzed the alignment of the CNT forests using image analysis techniques to calculate the alignment parameter (Φ). This is implemented with the "Directionality" plugin in the Fiji³⁴ open

source image analysis platform. This plugin is used to infer the preferred orientation of structures present in an input image.³⁵ When implemented in an SEM image, a histogram is generated indicating the frequency of structures in a given direction. This technique is based on the 2D fast Fourier transform technique, in which an image is decomposed into its spatial frequency components. Based on the resulting spectrum, the dominant alignments and spacings in a 2D image are estimated and tabulated into a histogram of angles. For example, SEM images with isotropic content generates a flat histogram, in contrast images with a preferred orientation produce a histogram with a peak identifying that orientation. From the histogram, the plugin reports the mean and standard deviation of the Gaussian fit of the histogram. The software fits the resulting histogram with a Gaussian function described by:

$$f(x) = a + (b - a) * e^{\left(-\frac{(x - \mu)^2}{2\sigma^2}\right)}$$
 (4)

where a and b are scaling parameters, μ is the mean and σ is the standard deviation of the Gaussian.

In this work, we define the reciprocal of the square of the computed standard deviation as the "Alignment Parameter" (Φ) :

$$\Phi = 1/\sigma^2. \tag{5}$$

In fact, this reciprocal of variance is defined as "precision" in statistics,³⁶ as it represents a clear measure of the sharpness of a distribution. It has also been utilized as a measure of precision in other research areas including bioinformatics and economics.^{37,38} Here, we employ this parameter as a quantitative metric describing the monodispersity of directionality of nanotubes. This parameter can have values between 0 and infinity, where 0 corresponds to random alignment and

infinity corresponds to perfect alignment.

3. RESULTS AND DISCUSSION

3.1. Decoupled growth recipes based on unique reactor capabilities

Complete decoupling of T_p, T_c, and T_g was enabled by our custom-designed multizone rapid thermal CVD reactor, schematically presented in Fig. 2a. 31,32 The reactor consists of two adjacent furnaces: a resistive preheater for gas-phase decomposition and an infrared (IR) heater for CNT growth. The carbon gas precursors are first thermally decomposed inside the preheater as they go through a coiled gas injector at temperature T_p. On the other hand, substrate temperature is controlled by the IR heater which is capable of rapidly changing the temperature from the catalyst formation temperature (T_c) during the catalyst treatment step in a reducing environment to the CNT growth temperature (T_o) during the CNT nucleation and growth step after introducing the carbon precursor at rates exceeding 50 °C/s. Hence, this unique design shown in Fig. 2a enables the complete decoupling of gas-phase decomposition, catalyst formation, and catalytic growth of CNTs, schematically depicted in Fig. 1. Moreover, growth is monitored in situ using a highdefinition video camera through a port that is designed to be along the quartz reactor tube axis. An example of camera view during a growth of CNT forest is shown as an inset in Fig. 2a. The *in situ* observation of growth enables us to detect the growth termination, so we can stop the growth step when the termination is detected.

It is often the case that there is a variation in height within a CNT forest. Typically, researchers

have reported the height of a CNT forest by a single measurement or by averaging the height measured from several points. To increase the accuracy of the measurement of height and volumetric mass density of a CNT forest, we used 3D optical microscopy to obtain an accurate digital imprint of forest geometry, as shown in Fig. 2b.

A typical decoupled recipe is displayed in Fig. 2c. The gas-phase hydrocarbon precursor molecules are decomposed while they travel through the preheater. In Fig. 2c, the red and blue solid lines represent the temperatures of the preheater and substrate (IR heated), respectively. Based on the dimensions of the coil shaped gas injector, the length of the preheater section and the flow rate of the gases injected through it, the residence time of the hydrocarbon precursor in the hot-wall preheater zone is calculated to be 10.4 seconds. Although the residence time of the gases traversing to the sample in the IR heated cold-wall zone is calculated to be 12.36 seconds, it should be noted that in the IR section, the gases do not heat up since they have poor absorptivity to IR radiation.³⁹ On the other hand, the residence time within the heated few millimeters around the substrate is calculated to be about 1 second. Hence, the residence time of the precursor gas in the preheater is an order of magnitude larger than the residence time around the IR-heated substrate. This quantitative comparison shows that the gas phase reactions are primarily taking place in the hotwall preheater zone of the reactor and negligible in the cold-wall IR zone.

It is also important to consider the possibility of recombination of pre-decomposed molecules. In our reactor, the short distance between the preheater and the IR heater minimizes this possibility of recombination, in contrast to reactor designs wherein the gases are allowed to cool down after coming out of the preheater before entering the growth reactor.²¹ Therefore, this design achieves close to ideal decoupling of gas-phase reaction from the surface catalytic reaction.

What enables the decoupling of catalyst formation step from growth step is the high heating/cooling rate by IR heating. While a similar approach was previously used, 28,29 our reactor is capable of faster heating with rates exceeding 50 °C/s and the cooling rate is also very high owing to the relatively small thermal mass (although it is dependent on temperature, as shown in Fig. S1). It is noteworthy that in conventional tube furnaces, T_c and T_g are coupled due to the inability to change the temperature rapidly owing to their large thermal mass. Hence, building on the advantage of rapid temperature control in our IR heater, we decoupled T_c from T_g . T_c can be lower (Fig. 2d) or higher (Fig. 2e) than T_g , or equal to T_g (Fig. 2f). In this work, we fixed all other experimental parameters such as the gas composition and the total flow rate.

3.2. Effects of decoupling on CNT forest height and density

When T_p was varied while fixing T_c and T_g (both at 620 °C), we observed that the height of CNT forests was highly dependent on T_p (Fig. 3a). When T_p was below 750 °C, the height was very small, but the height dramatically increased as T_p increased to above 800 °C. The high sensitivity of the height to T_p agrees with previous work in literature, 24 indicating the successful decoupling of gas-phase reactions from catalytic growth of CNTs in the main reactor, because T_p becomes higher than the thermal decomposition temperature of the precursor (C_2H_4 in our case). Hence, for a fixed T_p , changing T_c and T_g enables unprecedented ability to study the separate effects of temperature on the catalyst formation process and the CNT growth process independent of gas phase decomposition process. Hence, we kept T_p constant at 825 °C for all the rest of the growth experiments carried out in this work.

Results for decoupling of catalyst formation temperature (T_c) from catalytic CNT growth temperatures (T_g) are shown in Fig. 3b-d. First noticeable observation is the dependence of height on T_g and T_c (Fig. 3b). Previously, it has been widely observed that height of a CNT forest is dependent on growth temperature. ^{12,21,40,41} In our work, we also observed a dependence of forest height on T_g , wherein for any T_c , there is an optimum T_g at which a maximum height is achieved. Also, our decoupled recipe enabled us to show that for the same T_g , the height was largely affected by T_c in such a way that a higher T_c generally produced a taller CNT forest. The difference in height can be explained by either a difference in growth rate or a difference in catalyst lifetimes. Hence, further analysis of growth kinetics is required, but it is beyond the scope of the present study focusing on nucleation density.

Unlike height, density of a CNT forest was insensitive to T_c . At T_g = 720 °C, when T_c was varied from 680 to 900 °C, the density was nearly invariant (Fig. 3c). In contrast, we found that density was highly dependent on T_g . The density showed a strong negative correlation with T_g (Fig. 3d). This trend was observed both in the coupled (T_c = T_g) and the decoupled recipes ($T_c \neq T_g$), regardless of T_c . These results uniquely demonstrate the importance of decoupling T_c and T_g in order to generate new insights into CNT nucleation and growth. It is generally accepted that density of a CNT forest directly correlates with the number density of catalyst nanoparticles, which can be affected by the catalyst formation temperature T_c . Conversely, our results show that the density of CNT forest is dependent on T_g rather than T_c . It is noteworthy that there has been no quantitative report on the dependence of CNT forest density on growth temperature even though there are papers that quantify forest density. 5,6,15,42,43 This highlights an important gap in literature that we aim to fill with our study.

3.3. Effect of decoupling on morphology and structure of CNT forests

The vertically aligned morphology of the as-grown CNT forests was observed by scanning electron microscopy (SEM), with some noticeable variation of alignment between forests grown at different T_g (Fig. S2), which generally demonstrate lower density and alignment for forests grown at higher temperatures. These observations are quantified and discussed later in details. A typical SEM image of a highly aligned and dense CNT forest grown at $T_c = T_g = 600$ °C is shown in Fig. 4a. To investigate how T_{g} and T_{c} affect CNT diameter and number of walls, we used transmission electron microscopy (TEM) to analyze CNTs from three forest samples grown at different combinations of T_c and T_g : ($T_c = 700 \, ^{\circ}\text{C}$, $T_g = 600 \, ^{\circ}\text{C}$), ($T_c = 700 \, ^{\circ}\text{C}$, $T_g = 700 \, ^{\circ}\text{C}$), and ($T_c = 900 \, ^{\circ}\text{C}$) °C, T_g = 700 °C). We collected measurements from at least 40 CNTs from each CNT forest (Fig. 4b and Fig. S3) and obtained the distribution of outer diameter (Fig. 4c-e) and the distribution of number of walls (Fig. 4f-h) from the TEM images. The distribution of outer diameter was fitted using a lognormal curve, from which we obtained mode of the distribution of outer diameters for comparing with other samples. Since the number of walls measurement is a discrete variable, the mode of the distribution to be used for comparison is taken to be the tallest bar in the histograms shown in Fig. 4 f-h. We compared the mode of outer diameter and number of walls, as seen in Fig. 4i, instead of mean, owing to the observed skewness of the distributions (Table S1), which was previously shown in literature to best fit CVD-grown CNT populations. 16,44 Results indicate that the mode of outer CNT diameter was largely similar when T_c was equal (Fig. 4c and d). However, when T_c was higher, the mode of outer diameter was larger than the others (Fig. 4e). In addition, the distribution was wider at higher T_c ; the standard deviation was 1.80 at ($T_c = 700$ °C, $T_g = 600$

°C), 1.67 at ($T_c = 700$ °C, $T_g = 700$ °C), and 2.07 at ($T_c = 900$ °C, $T_g = 700$ °C). The mode of distribution for number of walls is also larger at ($T_c = 900$ °C, $T_g = 700$ °C) than at ($T_c = 700$ °C, $T_g = 700$ °C), and has a wider distribution as well. These observations of combined increase in both diameter and number of walls along with their wider distributions for higher T_c are consistent with the expected faster progression of Ostwald ripening at higher temperature. TEM results also show that CNTs growth with higher T_c (900 °C) show evidence of metal catalyst along the CNTs both inside and outside the CNTs as shown in Fig. S3c, which may be resulting from the higher catalyst mobility at higher T_c .

From the measured outer diameter and number of walls, we calculated areal number density of CNTs in the three samples using the following equation:

$$\rho_n = \frac{\rho_m/\rho_g}{\frac{\pi}{4}(d_o^2 - d_i^2)}$$
 (1)

where ρ_n is areal number density of CNTs, ρ_m is volumetric number density, ρ_g is density of graphite (2.2 g/cm³), d_o and d_i are outer and inner diameter of CNTs.⁴⁷ d_i was obtained from d_o and number of walls (n) according to the following formula:

$$d_i = d_0 - 0.68(n-1) \tag{2}$$

The calculated areal number density of CNTs is plotted in red in Fig. 4i. Since the outer and inner diameters of CNTs in the three samples were not very different, the areal number density showed a similar trend with volumetric mass density (Fig. 3d). Therefore, we demonstrate that both the areal number density and the mass density of CNT forests are negatively correlated to T_g and are nearly independent on T_c . Considering that the areal number density is determined at the nucleation

stage, it is reasonable to infer that the temperature at the nucleation stage influences the number of actively growing CNTs relative to the total number of nanoparticles, i.e. the catalyst activation percentage. Hence, it is important to characterize the catalyst nanoparticles size distributions.

3.4. Effect of decoupling T_c on catalyst nanoparticles

It is generally accepted that the size distribution and the areal number density of CNTs is determined by that of catalyst nanoparticles seeding their growth.^{5,6,18} To check the effect of T_c on the size and areal number density of catalyst nanoparticles, we analyzed the surface of the catalystcoated substrates using atomic force microscopy (AFM) after thermal treatments at three different catalyst formations temperatures. All substrates shown in Fig. 5 underwent the same catalyst formation step as in the growth recipe shown in Fig. 2c, but at different T_c (500, 700, and 900 °C) for 60 seconds. Then, the temperatures were ramped to 700 °C in 20 seconds, followed by cooling down to room temperature without proceeding to the growth step. In the case of $T_c = 700$ °C, the substrate stayed at 700 °C for 80 seconds. For each sample, we took three AFM images (Fig. 5a-c and Fig. S4) and analyzed the population of nanoparticles formed. The distributions of height of nanoparticles are plotted in Fig. 5d. The nanoparticles formed at higher T_c had larger heights (mean as well as mode of height distribution) and exhibited wider distribution, as seen in the plot in Fig. 5e and Table S2, which agrees with the larger outer diameter of CNTs grown with higher T_c (Fig. 4e) and previous reports, ^{28,46} because of faster Ostwald ripening at higher temperature. ⁴⁵

Interestingly, in all cases, there were sufficiently high areal number densities of nanoparticles, which were much higher than those of CNTs (approximately one order of magnitude higher), as

shown in Fig. 5e. Therefore, the trends of CNT density presented in Figs. 3 and 4 are not primarily limited by the areal number density of catalyst nanoparticles. Importantly, the difference in areal number density of nanoparticles between the three samples shown in Fig. 5 is relatively small compared to the difference in areal number density of CNTs shown in Fig, 4. This indicates that, even if the areal number densities of catalyst nanoparticles (ρ_c) are similar at the beginning of the growths, the areal number density of CNTs (ρ_n) can dramatically vary depending on T_g, which is a new insight derived from our decoupled growth approach. Although a higher areal number density of catalyst nanoparticles (ρ_c) is a necessary condition for a higher CNT nucleation density, it is not a sufficient condition, highlighting the importance of understanding what governs catalyst activation among large populations of substrate-bound nanoparticles.

The key to elucidating the reason for the dependence of areal number density of CNTs on T_g lies in the dependence of catalyst activation percentage (proportion of catalyst nanoparticles that end up successfully growing CNTs) on T_g , or, more accurately, on temperature at which CNT nucleation and lift-off takes place. Based on the areal number density of CNTs (ρ_n) obtained from weight gain measurements and TEM images (Fig. 4i) and the areal density of catalyst nanoparticles (ρ_c) measured from AFM images (Fig. 5e), we calculated the catalyst activation percentage (η), plotted in Fig. 5f:

$$\eta = \frac{\rho_n}{\rho_c} \times 100\%. \tag{3}$$

It is noteworthy that the catalyst activation percentage (η) as defined above may be also called CNT nucleation percentage or the success rate of CNT activation. Also, we have avoided the use of the term catalytic efficiency here, as it is less accurate and may confuse the reader in the context

of CNT population growth. Due to the similar areal number density of catalyst nanoparticles at T_c = 700 and 900 °C, CNT activation percentage showed a similar trend to the areal number density of CNTs with a high η (~ 40%) for (T_c = 700 °C, T_g = 600 °C) compared to the low η : 15.9% for (T_c = 700 °C, T_g = 700 °C) and 11.4% for (T_c = 900 °C, T_g = 700 °C).

Reporting accurate η requires a large number of measurements of CNT diameters by TEM, which becomes infeasible for large experimental sets. Hence, it is challenging to report accurate η values at multiple combinations of T_c and T_g . Nevertheless, based on the observation that the diameters do not vary significantly as a function of T_g , we estimated η at multiple sets of T_c and T_g , as shown in Fig. S5. Results highlight the inverse relationship between η and T_g with more than four-fold decrease of η as T_g increases from 600 to 720 °C (for T_c = 700 °C). Thus, it is clear that catalyst activation percentage (η) is inversely proportional to the temperature at which CNTs nucleate and grow (T_g), which is a new insight enabled by our decoupled process that has not been reported in prior studies.

It is important to note that only a few previous studies have reported values for catalyst activation percentage. For example, a value of 10% was previously reported for forests of multi-walled CNTs (MWCNTs). ¹⁶ In the case of single-walled CNT (SWCNT) forest growth, although there are several papers reporting CNT areal number density, ⁶ activation percentage is typically not reported with a single exception that reported a rather high value of 84%. ¹⁵ Ishida et al. also reported 10% catalyst activation percentage in the growth of SWCNTs, but in that study, catalyst nanoparticles were located far from each other and they did not form an aligned forest. ⁴⁸

3.5. Effect of decoupling T_g on the initial stage of growth: CNT nucleation and early growth

In order to better understand how changing T_g affects the early stage of CNT nucleation and growth, we study CNTs grown for short time at various T_g . For this purpose, we grew CNTs at a wide range of T_g (450, 550, 650, 750, and 850 °C) for a fixed short time (2 min) at a constant T_c and T_p of 500 and 825 °C, respectively. Results are summarized in Fig. 6 with SEMs showing the conditions that resulted in aligned forest growth (T_g = 550, 650, and 750 °C) and those that only resulted in either non-CNT carbonaceous particles at T_g = 450 °C, as shown in Fig. 6a and b, or resulted in tangled CNTs at T_g = 850 °C, as shown in Fig. 6c and d. Forest heights obtained from SEM (Fig. S6) are plotted in Fig. 6e, along with the ratio of G-band intensity to D-band intensity (I_G/I_D ratio) obtained from Raman spectroscopy. In addition, we calculated an alignment parameter (Φ), as a quantitative measure of the degree of vertical orientation of CNTs in forests based on Fourier component analysis of SEM images of the forest sidewalls, as shown in Fig. 6f-k (more details in the Experimental Methods section), and plot it in in Fig. 6e. Raman spectra corresponding to all growth results at all five T_g values are shown in Fig. 6l-p.

When T_g was 450 °C, no CNTs were grown, as shown in the SEM images in Fig. 6a, b, and in the corresponding Raman spectrum in Fig. 6l, in which weak G and D peaks were observed. These peaks are possibly arising from the formation of irregular carbonaceous particles or coating that while being largely amorphous may have some small graphitic content. For the successful nucleation of CNTs, high quality carbon caps need to be formed in order to lift off from the catalyst, but at low temperature, the energy supplied is not high enough and leads to low quality carbon formation and encapsulation of catalyst nanoparticles.^{49,50}

When T_g was between 550 and 750 °C, CNTs were densely grown to form a well-aligned forest structure (Fig. 6f-h). From the SEM images, we observe that the alignment of CNTs seems to be lower at higher T_g . By quantifying the alignment of CNTs using the directionality analysis based on Fourier spectra, we clearly demonstrate this comparison in the histograms showing the distribution of CNTs with specific angles of orientation (directions), as seen in Fig. 6 i-k. Moreover, when we calculate alignment parameter (Φ) based on the spread of those directionality histograms, we confirmed that the alignment decreases with T_g (Fig. 6i-k and Table S3). Since there is a positive correlation between alignment and the number density of CNTs that has been previously shown, 16,47,51 we can use the measured decrease of alignment parameter with T_g as a strong proxy for a decrease of density of CNTs with T_g . Thus, the inverse relation between mass density of CNT forests and T_g observed in Fig. 3d is also observed at the initial stage of the growth, proving that CNT nucleation density is also inversely proportional to the temperature of nucleation and growth (T_g) .

In this range of T_g , the growth time of 2 minutes is short enough to be confident that the growth experiments were stopped before reaching self-termination in all cases (i.e. at different T_g). Thus, the height of CNT forests grown for 2 minutes can be used as a measure of the initial growth rate. Our results show that the growth rate increased with T_g , which agrees with what is expected of an Arrhenius-type behavior (Fig. S7). I_G/I_D ratio also increased with T_g (Fig. 6l-p), indicating a marked enhancement of CNT quality for CNTs grown at higher temperatures, which is expected based on the likelihood of annealing defects at higher growth temperatures (Note that T_g is the temperature for both the nucleation and growth steps.). 52,53 We also quantitatively compared the purity (x) of CNTs – ratio of amorphous carbon content to CNT content in the sample – using the

following empirical formula⁵⁴:

$$\frac{I_D}{I_C} = 0.96 - 0.0066x \tag{4}$$

Using this equation, we evaluate the purity of the CNT forests grown for 2 minutes (shown in Fig 6) at various growth temperatures ($T_g = 550$ °C, 650 °C, and 750 °C) giving purity values of 94.82%, 95.54%, and 97.8% respectively. These support the interpretation that less amorphous carbon is accumulated at high T_g . Interestingly, at $T_g = 750$ °C, a sharp radial breathing mode (RBM) peak is observed in Fig. 6o, indicating that this forest is dominated by SWCNTs. Hence, in addition to enhancement of CNT crystallinity and purity with increasing T_g , our results suggest that these effects are concomitant with a transition towards promoting SWCNT growth.

When T_g was 850 °C, CNTs were grown so sparsely that they cannot form a forest structure, as seen in the top SEM view of the tangled CNT mat in Fig. 6b. Although it was difficult to measure the growth rate because they did not form a vertically aligned forest structure, it is expected that those few grown CNTs would have grown at a higher growth rate than at $T_g = 750$ °C. The grown CNTs included SWCNTs as confirmed by the RBM peak and had a relatively high I_G/I_D ratio (higher than for $T_g \le 650$ °C). Overall, at the same T_c , as T_g increases, nucleation density decreases while crystallinity and growth rate increases.

3.6. Mechanism explaining CNT nucleation dependence on $T_{\rm g}$

In order to explain the decrease of CNT activation percentage with increasing T_g , we need to consider the stochastic nature of CNT nucleation and population growth dynamics governing 10s-

100s of billions of CNTs making up a 1 centimeter squared area of forest. Although the growth of CNT forest has been often assumed to be uniform for simplification, it is actually governed by the distributions of catalyst nanoparticles in terms of diameter, shape, and physical/chemical state.

4,11,44 Thus, as shown in Fig. 7, we hypothesize that the lower CNT nucleation percentage at higher T_g is because CNT growth at each catalyst nanoparticle has different activation energy, and consequently different growth rate,⁵⁵ which is dependent on it size, shape and/or phase.

Although the concentration of active carbon species in the bulk flow may be high enough, the diffusion flux through the diffusion boundary layer determines the growth kinetics. In fact, it has been shown that the growth can be shifted from reaction-limited to diffusion-limited condition as temperature increases. Hence, we should consider the concentration profile in the diffusion boundary layer. The spatial distribution of catalyst nanoparticles leads to local depletion of active carbon species around specific catalyst nanoparticles, which rapidly consume the local supply of those active species owing to their fast growth kinetics. As a result, other neighboring catalyst nanoparticles could starve as they compete with those "greedy" nanoparticles that siphon off a greater share of the available active species in the diffusion boundary layer. Hence, for the same partial pressures, the precursor supply can support only a smaller number of catalyst nanoparticles for fast-growing CNTs at higher T_g.

For successful activation of catalyst nanoparticles, proper feeding of carbon is important. For example, Lu *et al.* reported that, given a carbon feeding rate, catalyst nanoparticles can be selectively activated depending on their size.⁵⁸ According to that report, when the nanoparticles are too small, they are overfed and thus are poisoned. On the contrary, when the nanoparticles are too large, they are underfed. Hence, that study emphasizes that the proper feeding rate of carbon

source is important in successful activation of catalyst nanoparticles.

At low T_g , since the growth rates are low in general, the gaseous carbon species are slowly consumed. The rate of the mass transport from the bulk gas phase through the boundary layer to the surface of catalyst nanoparticles is sufficient, so the carbon species can be evenly supplied to many catalyst nanoparticles. However, at a higher T_g , higher growth rates lead to local nonuniformity in the concentration of carbon species. This nonuniformity is exacerbated by the greater hindrance to mass transport through the thicker boundary layer at higher T_g , whose thickness varies with the temperature-dependent gas viscosity.⁵⁹

It has been proposed before that the growth rate of each CNT is different depending on CNT chirality, ^{60,61} or the size and composition of catalyst nanoparticles. ^{44,62,63} At a higher T_g, some catalyst nanoparticles that have relatively low activation energy can produce CNTs at much higher rates. If they nucleate CNTs earlier than others and continue to grow CNTs, they will monopolize the carbon species around them, causing local depletion of carbon species. Carbon species in the vicinity of the substrate will tend to be exclusively incorporated in CNTs that are growing from the "surviving" catalyst nanoparticles by following the low-activation-energy path, rather than activate new high-activation-energy catalyst nanoparticles.

With the decrease of density at an even higher T_g , we find that both number of walls and diameter also decrease underpinning the eventual shift toward growing SWCNTs as shown in Fig. 6. This can also be explained in the framework of our proposed local depletion mechanism. At this high T_g , the growth rate is so fast that the growth can be easily limited by diffusion. In the diffusion-limited situation, the catalysts are no longer able to eject enough carbon atoms to form the multi-

walled CNTs. Alternatively, the catalysts produce CNTs having smaller diameter, fewer walls (or single wall). In fact, Smalley *et al.* have previously reported that the transition from reaction-limited to diffusion-limited growth causes selective synthesis of SWCNTs.⁶⁴ In addition, Liu *et al.* have shown that CNT diameter decreases even from the same catalyst nanoparticle when temperature increases, which is consistent with our hypothesis.^{65,66} From the perspective of population growth dynamics, it has been shown before that the diameter distribution of a forest shift towards a smaller diameter as the forest evolves towards growth self-termination, concomitant with progressive deactivation of catalyst nanoparticle subpopulations with larger diameter (i.e. larger CNTs "die" first).^{16,44}

The outer diameter and number of walls in Fig. 4 can be explained with the proposed hypothesis. When we compare the growths at $T_c = 700$ °C, the mode of number of walls was lower at higher T_g (Fig. 4f, g), although the modes of outer diameters were similar (Fig. 4c, d). The outer diameters were similar because catalyst nanoparticles are formed at the same T_c , but at higher T_g , the consumption of carbon is faster while the supply of active carbon species is the same. As a result, CNTs with smaller number of walls are produced.

Although we propose the "local depletion" as a mechanism for the T_g-dependence of catalyst activation percentage, we also consider other mechanisms such as catalyst poising by either the formation of an inactive phase (e.g. iron carbide⁶⁷ or iron oxide^{19,68}), or the encapsulation of catalyst nanoparticles by conformal deposition of a carbon layer.^{49,50,69} First, according to the literature, iron carbide is energetically unfavorable at higher temperature, so iron carbide would break down more at higher T_g.⁶⁷ Thus, it is unlikely that the portion of iron carbide among catalyst nanoparticle population increases at higher T_g. Second, since the growth is under reducing

environment, oxidation would not be promoted at higher T_g , which rules out the formation of less active iron oxide phases with increasing T_g . Finally, it has been observed that catalyst nanoparticles become inactive as a result of coating by a graphitic shell.²⁰ However, the effect of temperature on the formation of graphitic coating is still a subject of on-going research. Molecular dynamics simulations by Ding *et al.*, predicted the graphitic encapsulation of catalyst nanoparticles at low temperature due to insufficient energy for the lift-off, ^{49,50} but experimental results for these effects are rather scarce. Thus, we cannot confidently rule out the possibility of having more encapsulation of carbon nanoparticles by graphitic shell at higher T_g , which was observed previously in environmental TEM studies of CNT nucleation and growth.^{17,20}

It is noteworthy that the independent effect of T_g can only be clearly demonstrated here because of our decoupled recipes enabled by our custom-designed multizone rapid thermal CVD reactor. In our decoupled recipes, the supply of gaseous carbon species is the same regardless of T_g as T_p is decoupled from T_g . If T_p is coupled to T_g , it is impossible to exclude the different supply of gaseous carbon species as any change of temperature inevitably causes different local concentration and chemistry of precursor gas. Besides, since we decoupled T_c from T_g , we can assume the formation of similar catalyst nanoparticle populations in terms of size distribution, same number density, and chemical state. Otherwise, without decoupling T_c , growth at different temperatures would also cause variations in the catalyst nanoparticles, which would make it difficult to explain what governs the activation percentage for similar catalyst nanoparticles. In fact, to the best of our knowledge, there has been little literature about the effect of growth temperature on density of CNTs, which is because of the intrinsic difficulty in independently investigating the effect of various parameters. Thus, we propose that our decoupled recipe is an

ideal approach to elucidate the independent effect of temperatures during (1) catalyst nanoparticle formation by thin film dewetting, (2) thermal decomposition of gas-phase precursors, and (3) nucleation and growth of CNTs on the catalytic surfaces of nanoparticles. Accordingly, our study provides insights into tailoring the density, size, alignment and quality of CNT forest growth for tuning their collective properties.

4. CONCLUSIONS

We successfully demonstrate the complete decoupling of both gas-phase decomposition and catalyst nanoparticle formation from the catalytic growth of CNTs in CVD. We achieve this by leveraging a custom-designed reactor equipped with a separate preheater and rapid thermal processing capability. Using the decoupled growth recipes, we revealed the dependence of areal number density of CNTs on nucleation temperature. We show that the decrease of areal number density of CNTs with increased nucleation temperature is not because of number density of catalyst nanoparticles, but because of a marked decrease of catalyst activation percentage. To explain this phenomenon, we propose a "local depletion" mechanism, wherein the growth rate at each catalyst nanoparticle is different, and at higher T_g, active carbon species are locally depleted around catalyst nanoparticles with faster growth rates. This spatial distribution causes starvation at other catalyst nanoparticles leading to the observed decrease in catalyst activation percentage. We believe that the complete decoupling approach introduced in this work is a powerful methodology that enables the independent investigation of catalyst preparation and CNT nucleation processes. Moreover, the access to a larger parameter space offered by our approach

opens the door toward unprecedented control on the morphology and collective properties of asgrown CNT forests for specific applications.

ACKNOWLEDGEMENTS

This research was supported by the National Science Foundation (NSF) under award number 1825772 (any opinions, findings, and conclusions or recommendations expressed in this material are those of the author(s) and do not necessarily reflect the views of the National Science Foundation). Work was also supported by the Department of Industrial Engineering at the University of Pittsburgh. M. Bedewy is grateful for the Ralph E. Powe Junior Faculty Enhancement Award from Oak Ridge Associated Universities (ORAU). Characterization was performed, in part, at the Nanoscale Fabrication and Characterization Facility, a laboratory of the Gertrude E. and John M. Petersen Institute of NanoScience and Engineering, housed at the University of Pittsburgh, and in part, at Materials Characterization Laboratory, housed at Department of Chemistry in the University of Pittsburgh.

SUPPORTING INFORMATION DESCRIPTION

Cooling curves of the reactor; SEM images of as-grown CNT forests; TEM images of as-grown CNTs; AFM images of catalyst nanoparticles; Estimated catalyst activation percentages as a function of growth temperature (T_g); SEM images of short forests grown for 2 minutes; Arrhenius plot of CNT growth; statistics of lognormal fitting of outer diameter of CNTs and catalyst

nanoparticle height; directionality analysis result of CNT forests

REFERENCES

- (1) Yu, M.; Yu, M.; Lourie, O.; Dyer, M. J.; Moloni, K.; Kelly, T. F.; Ruoff, R. S. Strength and Breaking Mechanism of Multiwalled Carbon Nanotubes Under Tensile Load. *Science* **2000**, *287* (2000), 637–640.
- (2) Berber, S.; Kwon, Y.-K.; Tomanek, D. Unusually High Thermal Conductivity of Carbon Nanotubes. *Phys. Rev. Lett.* **2000**, *84* (20), 4613–4616.
- (3) Ebbesen, T. W.; Lezec, H. J.; Hiura, H.; Bennett, J. W.; Ghaemi, H. .; Thio, T. Electrical Conductivity of Individual Carbon Nanotubes. *Nature*. 1996, pp 54–56.
- (4) Bedewy, M. Data-Driven Understanding of Collective Carbon Nanotube Growth by in Situ Characterization and Nanoscale Metrology. *J. Mater. Res.* **2017**, *32* (01), 153–165.
- (5) Esconjauregui, S.; Fouquet, M.; Bayer, B. C.; Ducati, C.; Smajda, R.; Hofmann, S.; Robertson, J. Growth of Ultrahigh Density Vertically Aligned Carbon Nanotube Forests for Interconnects. *ACS Nano* **2010**, *4* (12), 7431–7436.
- (6) Zhong, G.; Warner, J. H.; Fouquet, M.; Robertson, A. W.; Chen, B.; Robertson, J. Growth of Ultrahigh Density Single-Walled Carbon Nanotube Forests by Improved Catalyst Design. ACS Nano 2012, 6 (4), 2893–2903.
- (7) Marconnet, A. M.; Panzer, M. A.; Goodson, K. E. Thermal Conduction Phenomena in Carbon Nanotubes and Related Nanostructured Materials. Rev. Mod. Phys. 2013, 85 (3),

1295-1326.

- (8) Kim, S.; Fornasiero, F.; Park, H. G.; In, J. Bin; Meshot, E.; Giraldo, G.; Stadermann, M.; Fireman, M.; Shan, J.; Grigoropoulos, C. P.; et al. Fabrication of Flexible, Aligned Carbon Nanotube/Polymer Composite Membranes by in-Situ Polymerization. *J. Memb. Sci.* 2014, 460, 91–98.
- (9) W. Z., G. L.; S. S., X.; Qian L.X.; B. H., C.; Zou B. S.; W. Y., Z.; Wang, Z. R. A. Large-Scale Synthesis of Aligned Carbon Nanotubes. *Science* 1996, 274 (5293), 1701–1703.
- (10) Fan, S.; Chapline, M. G.; Franklin, N. R.; Tombler, T. W.; Cassell, A. M.; Dai, H. Self-Oriented Regular Arrays of Carbon Nanotubes and Their Field Emission Properties.
 Science 1999, 283 (5401), 512–514.
- (11) Bedewy, M.; Meshot, E. R.; Reinker, M. J.; Hart, A. J. Population Growth Dynamics of Carbon Nanotubes. *ACS Nano* **2011**, *5* (11).
- (12) Cho, W.; Schulz, M.; Shanov, V. Growth and Characterization of Vertically Aligned Centimeter Long CNT Arrays. *Carbon* **2014**, *72*, 264–273.
- (13) Lee, J.; Oh, E.; Kim, T.; Sa, J. H.; Lee, S. H.; Park, J.; Moon, D.; Kang, I. S.; Kim, M. J.; Kim, S. M.; et al. The Influence of Boundary Layer on the Growth Kinetics of Carbon Nanotube Forests. *Carbon* **2015**, *93*, 217–225.
- (14) Yamazaki, Y.; Katagiri, M.; Sakuma, N.; Suzuki, M.; Sato, S.; Nihei, M.; Wada, M.; Matsunaga, N.; Sakai, T.; Awano, Y. Synthesis of a Closely Packed Carbon Nanotube Forest by a Multi-Step Growth Method Using Plasma-Based Chemical Vapor Deposition.

- Appl. Phys. Express 2010, 3 (5), 055002.
- (15) Futaba, D. N.; Hata, K.; Namai, T.; Yamada, T.; Mizuno, K.; Hayamizu, Y.; Yumura, M.; Iijima, S. 84% Catalyst Activity of Water-Assisted Growth of Single Walled Carbon Nanotube Forest Characterization by a Statistical and Macroscopic Approach. *J. Phys. Chem. B* 2006, *110* (15), 8035–8038.
- (16) Bedewy, M.; Meshot, E. R.; Reinker, M. J.; Hart, A. J. Population Growth Dynamics of Carbon Nanotubes. *ACS Nano* **2011**, *5* (11), 8974–8989.
- (17) Balakrishnan, V.; Bedewy, M.; Meshot, E. R.; Pattinson, S. W.; Polsen, E. S.; Laye, F.; Zakharov, D. N.; Stach, E. A.; Hart, A. J. Real-Time Imaging of Self-Organization and Mechanical Competition in Carbon Nanotube Forest Growth. *ACS Nano* 2016, *10* (12), 11496–11504.
- (18) Meshot, E. R.; Verploegen, E.; Bedewy, M.; Tawfick, S.; Woll, A. R.; Green, K. S.; Hromalik, M.; Koerner, L. J.; Philipp, H. T.; Tate, M. W.; et al. High-Speed in Situ X-Ray Scattering of Carbon Nanotube Film Nucleation and Self-Organization. *ACS Nano* 2012, 6 (6), 5091–5101.
- (19) Mattevi, C.; Wirth, C. T.; Hofmann, S.; Blume, R.; Cantoro, M.; Ducati, C.; Cepek, C.; Knop-Gericke, A.; Milne, S.; Castellarin-Cudia, C.; et al. In-Situ X-Ray Photoelectron Spectroscopy Study of Catalyst–Support Interactions and Growth of Carbon Nanotube Forests. *J. Phys. Chem. C* 2008, *112* (32), 12207–12213.
- (20) Bedewy, M.; Viswanath, B.; Meshot, E. R.; Zakharov, D. N.; Stach, E. A.; Hart, A. J.

- Measurement of the Dewetting, Nucleation, and Deactivation Kinetics of Carbon Nanotube Population Growth by Environmental Transmission Electron Microscopy. *Chem. Mater.* **2016**, *28* (11), 3804–3813.
- (21) Meshot, E. R.; Plata, D. L.; Tawfick, S.; Zhang, Y.; Verploegen, E. a; Hart, a J. Engineering Vertically Aligned Carbon Nanotube Growth by Decoupled Thermal Treatment of Precursor and Catalyst. ACS Nano 2009, 3 (9), 2477–2486.
- (22) Nessim, G. D.; Seita, M.; Plata, D. L.; OBrien, K. P.; John Hart, A.; Meshot, E. R.; Reddy, C. M.; Gschwend, P. M.; Thompson, C. V. Precursor Gas Chemistry Determines the Crystallinity of Carbon Nanotubes Synthesized at Low Temperature. *Carbon* 2011, 49 (3), 804–810.
- (23) Lee, C. J.; Son, K. H.; Park, J.; Yoo, J. E.; Huh, Y.; Lee, J. Y. Low Temperature Growth of Vertically Aligned Carbon Nanotubes by Thermal Chemical Vapor Deposition. *Chem. Phys. Lett.* **2001**, *338* (2–3), 113–117.
- (24) Nessim, G. D.; Seita, M.; O'Brien, K. P.; Hart, A. J.; Bonaparte, R. K.; Mitchell, R. R.; Thompson, C. V. Low Temperature Synthesis of Vertically Aligned Carbon Nanotubes with Electrical Contact to Metallic Substrates Enabled by Thermal Decomposition of the Carbon Feedstock. *Nano Lett.* **2009**, *9* (10), 3398–3405.
- (25) Jeong, H. J.; Jeong, S. Y.; Shin, Y. M.; Han, J. H.; Lim, S. C.; Eum, S. J.; Yang, C. W.; Kim, N. G.; Park, C. Y.; Lee, Y. H. Dual-Catalyst Growth of Vertically Aligned Carbon Nanotubes at Low Temperature in Thermal Chemical Vapor Deposition. *Chem. Phys. Lett.* 2002, 361 (3–4), 189–195.

- (26) Youn, S. K.; Frouzakis, C. E.; Gopi, B. P.; Robertson, J.; Teo, K. B. K.; Park, H. G. Temperature Gradient Chemical Vapor Deposition of Vertically Aligned Carbon Nanotubes. *Carbon* **2013**, *54*, 343–352.
- (27) Yang, N.; Youn, S. K.; Frouzakis, C. E.; Park, H. G. An Effect of Gas-Phase Reactions on the Vertically Aligned CNT Growth by Temperature Gradient Chemical Vapor Deposition. *Carbon* **2018**, *130*, 607–613.
- (28) Sakurai, S.; Inaguma, M.; Futaba, D. N.; Yumura, M.; Hata, K. Diameter and Density Control of Single-Walled Carbon Nanotube Forests by Modulating Ostwald Ripening through Decoupling the Catalyst Formation and Growth Processes. *Small* **2013**, *9* (21), 3584–3592.
- (29) Sakurai, S.; Inaguma, M.; Futaba, D. N.; Yumura, M.; Hata, K. A Fundamental Limitation of Small Diameter Single-Walled Carbon Nanotube Synthesis-a Scaling Rule of the Carbon Nanotube Yield with Catalyst Volume. *Materials (Basel)*. **2013**, *6* (7), 2633–2641.
- (30) Li, J.; Bedewy, M.; White, A. O.; Polsen, E. S.; Tawfick, S.; John Hart, A. Highly Consistent Atmospheric Pressure Synthesis of Carbon Nanotube Forests by Mitigation of Moisture Transients. *J. Phys. Chem. C* **2016**, *120* (20), 11277–11287.
- (31) Lee, J.; Abdulhafez, M.; Bedewy, M. Data Analytics Enables Significant Improvement of Robustness in Chemical Vapor Deposition of Carbon Nanotubes Based on Vacuum Baking. *Ind. Eng. Chem. Res.* 2019, 58 (27), 11999–12009.
- (32) Lee, J.; Abdulhafez, M.; Bedewy, M. Multizone Rapid Thermal Processing to Overcome

- Challenges in Carbon Nanotube Manufacturing by Chemical Vapor Deposition. *J. Manuf. Sci. Eng.* **2019**, *141* (9), 091006.
- (33) Lee, J.; Lee, C. H.; Park, J.; Lee, D. M.; Lee, K. H.; Jo, S. B.; Cho, K.; Maruyama, B.; Kim, S. M. Effects of a SiO2 Sub-Supporting Layer on the Structure of a Al2O3 Supporting Layer, Formation of Fe Catalyst Particles, and Growth of Carbon Nanotube Forests. *RSC Adv.* 2016, 6 (72), 68424–68432.
- (34) Schindelin, J.; Arganda-Carreras, I.; Frise, E.; Kaynig, V.; Longair, M.; Pietzsch, T.; Preibisch, S.; Rueden, C.; Saalfeld, S.; Schmid, B.; et al. Fiji: An Open-Source Platform for Biological-Image Analysis. *Nat. Methods* **2012**, *9* (7), 676–682.
- (35) Sensini, A.; Gualandi, C.; Zucchelli, A.; Boyle, L. A.; Kao, A. P.; Reilly, G. C.; Tozzi, G.; Cristofolini, L.; Focarete, M. L. Tendon Fascicle-Inspired Nanofibrous Scaffold of Polylactic Acid/Collagen with Enhanced 3D-Structure and Biomechanical Properties. *Sci. Rep.* **2018**, *8* (1), 1–15.
- (36) Dodge, Y. The Oxford Dictionary of Statistical Terms; Oxford University Press, 2003.
- (37) Jelliffe, R. W.; Schumitzky, A.; Bayard, D.; Fu, X.; Neely, M. Describing Assay

 Precision—Reciprocal of Variance Is Correct, Not CV Percent. *Ther. Drug Monit.* **2015**, 37 (3), 389–394.
- (38) Arrow, K. J. The Economics of Information: An Exposition. *Empirica* **1996**, *23* (2), 119–128.
- (39) Gupta, M.; Leong, E. W. W. Microwaves and Metals; John Wiley & Sons: Hoboken, NJ,

USA, 2007.

- (40) Puretzky, A. A.; Geohegan, D. B.; Jesse, S.; Ivanov, I. N.; Eres, G. In Situ Measurements and Modeling of Carbon Nanotube Array Growth Kinetics during Chemical Vapor Deposition. *Appl. Phys. A* **2005**, *81* (2), 223–240.
- (41) Huynh, C. P.; Hawkins, S. C. Understanding the Synthesis of Directly Spinnable Carbon Nanotube Forests. *Carbon* **2010**, *48* (4), 1105–1115.
- (42) Nessim, G. D.; Hart, A. J.; Kim, J. S.; Acquaviva, D.; Oh, J.; Morgan, C. D.; Seita, M.; Leib, J. S.; Thompson, C. V. Tuning of Vertically-Aligned Carbon Nanotube Diameter and Areal Density through Catalyst Pre-Treatment. *Nano Lett.* **2008**, *8* (11), 3587–3593.
- (43) Zhong, G. F.; Iwasaki, T.; Kawarada, H. Semi-Quantitative Study on the Fabrication of Densely Packed and Vertically Aligned Single-Walled Carbon Nanotubes. *Carbon* 2006, 44 (10), 2009–2014.
- (44) Bedewy, M.; Meshot, E. R.; Hart, A. J. Diameter-Dependent Kinetics of Activation and Deactivation in Carbon Nanotube Population Growth. *Carbon* **2012**, *50* (14), 5106–5116.
- (45) Wynblatt, P. Particle Growth in Model Supported Metal Catalysts-II. Comparison of Experiment with Theory. *Acta Metall.* **1976**, *24* (12), 1175–1182.
- (46) Kim, S. M.; Pint, C. L.; Amama, P. B.; Zakharov, D. N.; Hauge, R. H.; Maruyama, B.; Stach, E. A. Evolution in Catalyst Morphology Leads to Carbon Nanotube Growth Termination. *J. Phys. Chem. Lett.* **2010**, *1* (6), 918–922.
- (47) Bedewy, M.; Meshot, E. R.; Guo, H.; Verploegen, E. A.; Lu, W.; Hart, A. J. Collective

- Mechanism for the Evolution and Self-Termination of Vertically Aligned Carbon Nanotube Growth. *J. Phys. Chem. C* **2009**, *113* (48).
- (48) Ishida, M.; Hongo, H.; Nihey, F.; Ochiai, Y. Diameter-Controlled Carbon Nanotubes
 Grown from Lithographically Defined Nanoparticles. *Japanese J. Appl. Physics, Part 2 Lett.* **2004**, *43* (10 B).
- (49) Ding, F.; Bolton, K.; Rosén, A. Nucleation and Growth of Single-Walled Carbon Nanotubes: A Molecular Dynamics Study. *J. Phys. Chem. B* 2004, *108* (45), 17369– 17377.
- (50) Ding, F.; Rosén, A.; Campbell, E. E. B.; Falk, L. K. L.; Bolton, K. Graphitic Encapsulation of Catalyst Particles in Carbon Nanotube Production. *J. Phys. Chem. B* 2006, 110 (15), 7666–7670.
- (51) Xu, M.; Futaba, D. N.; Yumura, M.; Hata, K. Alignment Control of Carbon Nanotube Forest from Random to Nearly Perfectly Aligned by Utilizing the Crowding Effect. *ACS Nano* **2012**, *6* (7), 5837–5844.
- (52) Lee, C. J.; Park, J.; Huh, Y.; Yong Lee, J. Temperature Effect on the Growth of Carbon Nanotubes Using Thermal Chemical Vapor Deposition. *Chem. Phys. Lett.* **2001**, *343* (1–2), 33–38.
- (53) Lee, Y. T.; Park, J.; Choi, Y. S.; Ryu, H.; Lee, H. J. Temperature-Dependent Growth of Vertically Aligned Carbon Nanotubes in the Range 800-1100 °C. *J. Phys. Chem. B* **2002**, *106* (31), 7614–7618.

- (54) DiLeo, R. A.; Landi, B. J.; Raffaelle, R. P. Purity Assessment of Multiwalled Carbon Nanotubes by Raman Spectroscopy. J. Appl. Phys. 2007, 101 (6), 064307.
- (55) Geohegan, D. B.; Puretzky, A. A.; Jackson, J. J.; Rouleau, C. M.; Eres, G.; More, K. L. Flux-Dependent Growth Kinetics and Diameter Selectivity in Single-Wall Carbon Nanotube Arrays. *ACS Nano* **2011**, *5* (10), 8311–8321.
- (56) Zhu, L.; Hess, D. W.; Wong, C. P. Monitoring Carbon Nanotube Growth by Formation of Nanotube Stacks and Investigation of the Diffusion-Controlled Kinetics. *J. Phys. Chem. B* 2006, 110 (11), 5445–5449.
- (57) Bedewy, M.; Farmer, B.; Hart, A. J. Synergetic Chemical Coupling Controls the Uniformity of Carbon Nanotube Microstructure Growth. *ACS Nano* **2014**, *8* (6), 5799–5812.
- (58) Lu, C.; Liu, J. Controlling the Diameter of Carbon Nanotubes in Chemical Vapor Deposition Method by Carbon Feeding. J. Phys. Chem. B 2006, 110 (41), 20254–20257.
- (59) Miller, R.; Garrett, S. J.; Griffiths, P. T.; Hussain, Z. Stability of the Blasius Boundary

 Layer over a Heated Plate in a Temperature-Dependent Viscosity Flow. *Phys. Rev. Fluids* **2018**, *3* (11), 113902.
- (60) Rao, R.; Liptak, D.; Cherukuri, T.; Yakobson, B. I.; Maruyama, B. In Situ Evidence for Chirality-Dependent Growth Rates of Individual Carbon Nanotubes. *Nat. Mater.* 2012, *11* (3), 213–216.
- (61) Liu, B.; Liu, J.; Tu, X.; Zhang, J.; Zheng, M.; Zhou, C. Chirality-Dependent Vapor-Phase

- Epitaxial Growth and Termination of Single-Wall Carbon Nanotubes. *Nano Lett.* **2013**, *13* (9), 4416–4421.
- (62) Li, H. B.; Page, A. J.; Irle, S.; Morokuma, K. Single-Walled Carbon Nanotube Growth from Chiral Carbon Nanorings: Prediction of Chirality and Diameter Influence on Growth Rates. *J. Am. Chem. Soc.* **2012**, *134* (38), 15887–15896.
- (63) Chiang, W. H.; Sankaran, R. M. Relating Carbon Nanotube Growth Parameters to the Size and Composition of Nanocatalysts. *Diam. Relat. Mater.* **2009**, *18* (5–8), 946–952.
- (64) Hafner, J. H.; Bronikowski, M. J.; Azamian, B. R.; Nikolaev, P.; Rinzler, A. G.; Colbert,
 D. T.; Smith, K. A.; Smalley, R. E. Catalytic Growth of Single-Wall Carbon Nanotubes
 from Metal Particles. *Chem. Phys. Lett.* 1998, 296 (1–2), 195–202.
- Yao, Y.; Li, Q.; Zhang, J.; Liu, R.; Jiao, L.; Zhu, Y. T.; Liu, Z. Temperature-Mediated
 Growth of Single-Walled Carbon-Nanotube Intramolecular Junctions. *Nat. Mater.* 2007, 6
 (4), 293–296.
- (66) Yao, Y.; Xiaochuan, D.; Liu, R.; Zhang, J.; Liu, Z. Tuning the Diameter of Single-Walled Carbon Nanotubes by Temperature-Mediated Chemical Vapor Deposition. *J. Phys. Chem.* C 2009, 113 (30), 13051–13059.
- (67) Mazzucco, S.; Wang, Y.; Tanase, M.; Picher, M.; Li, K.; Wu, Z.; Irle, S.; Sharma, R.
 Direct Evidence of Active and Inactive Phases of Fe Catalyst Nanoparticles for Carbon
 Nanotube Formation. J. Catal. 2014, 319, 54–60.
- (68) Hofmann, S.; Blume, R.; Wirth, C. T. C. T.; Cantoro, M.; Sharma, R.; Ducati, C.;

Hävecker, M.; Zafeiratos, S.; Schnoerch, P.; Oestereich, A.; et al. State of Transition Metal Catalysts During Carbon Nanotube Growth. *J. Phys. Chem. C* **2009**, *113* (5), 1648–1656.

(69) Bedewy, M.; Viswanath, B.; Meshot, E. R.; Zakharov, D. N.; Stach, E. A.; Hart, A. J. Measurement of the Dewetting, Nucleation, and Deactivation Kinetics of Carbon Nanotube Population Growth by Environmental Transmission Electron Microscopy. *Chem. Mater.* 2016, 28 (11).

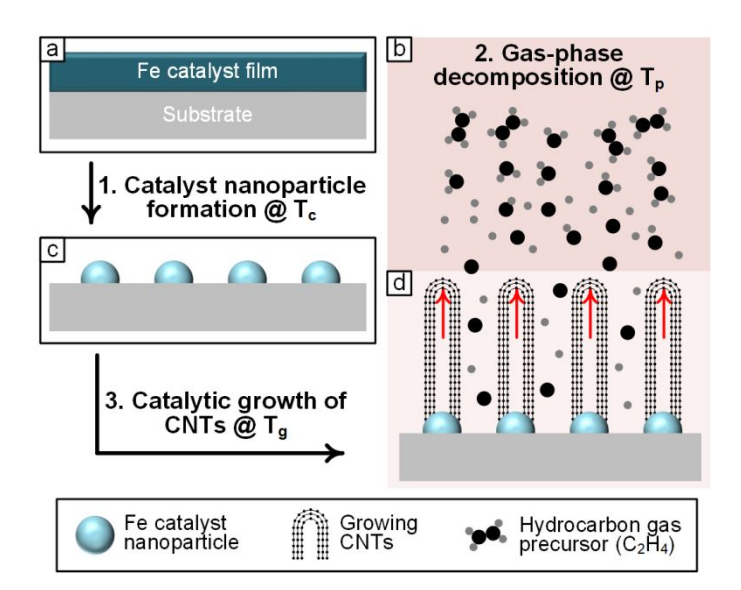


Fig. 1. Schematic representation of decoupling the catalyst formation temperature (T_c) , the gas decomposition temperature (T_p) and the growth temperature (T_g) in CVD of CNTs. (a) As deposited catalyst thin film. (b) Gas-phase decomposition in the preheater at T_p . (c) Thin film reduction and dewetting to form catalyst nanoparticles at T_c . (d) CNT nucleation and growth from active catalyst at T_g .

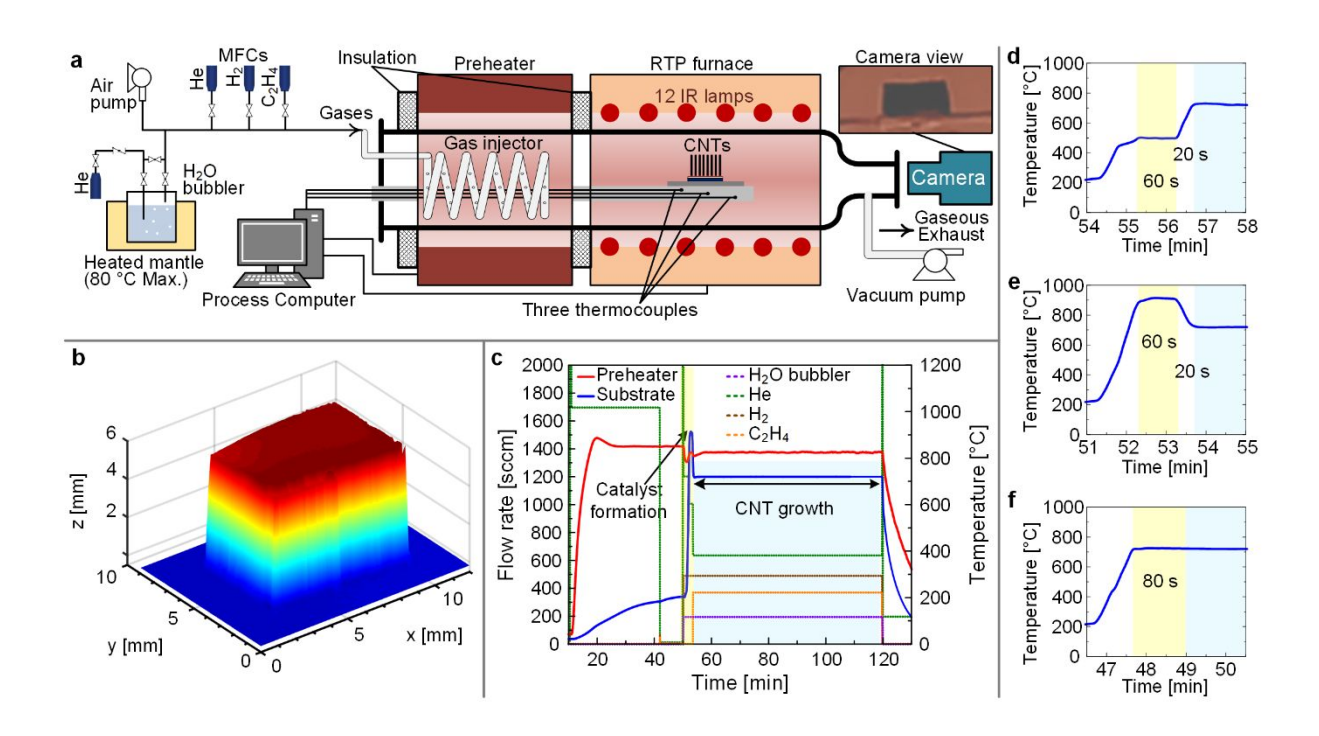


Fig. 2. (a) Schematic representation of the multizone RTP CVD reactor used in this work. (b) Accurate digital 3D data for forest geometry obtained by 3D optical microscopy. (c) A typical decoupled growth recipe showing the temperatures and gas follow rates. (d) – (f) Three types of temperature sequences in which (d) $T_c < T_g$, (e) $T_c > T_g$, and (f) $T_c = T_g$.

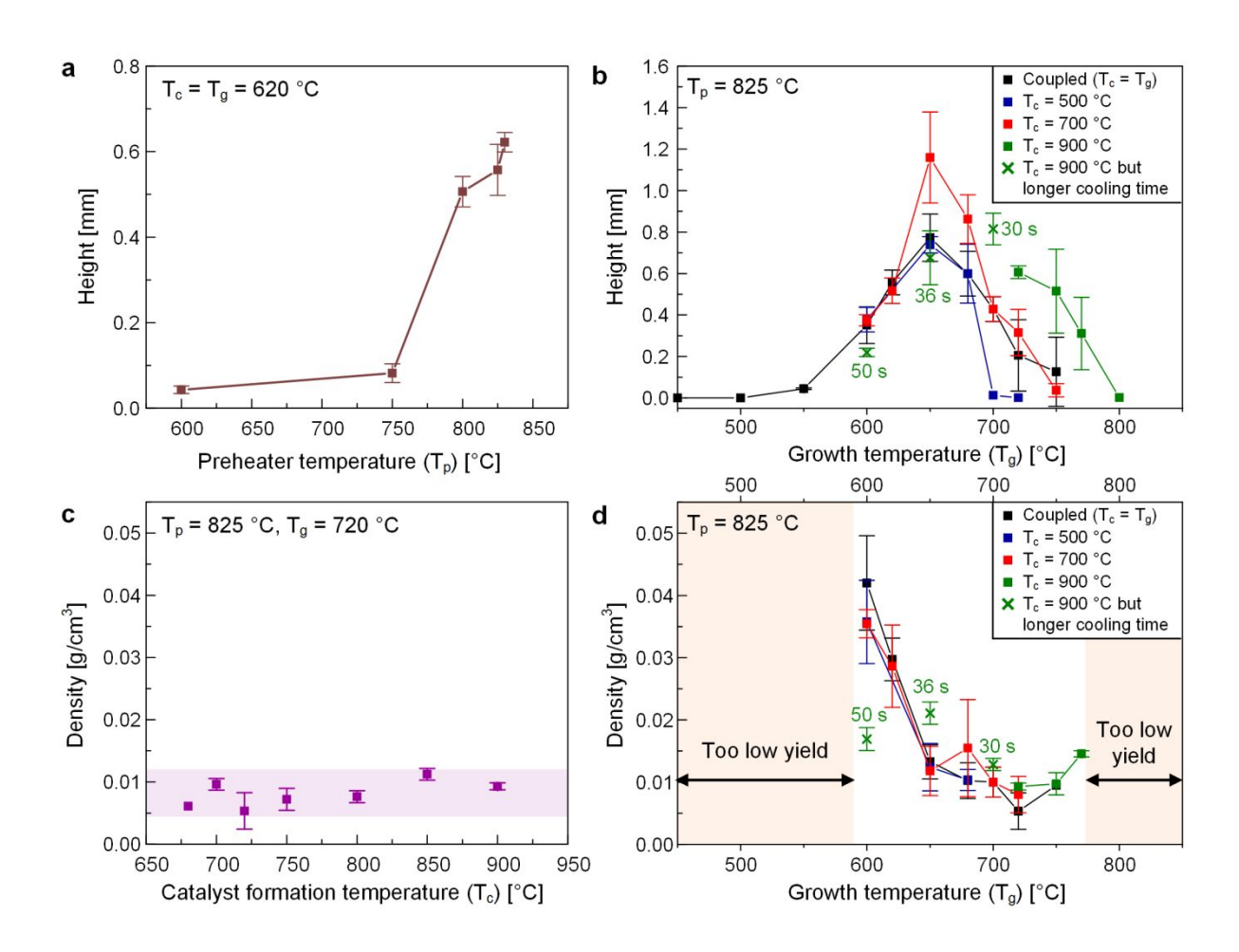


Fig. 3. Effects of decoupling on height and density of CNT forest: (a) height as a function of preheater temperature T_p , (b) height dependence on catalyst formation temperature T_c and growth temperature T_g , (c) density dependence on T_c , and (d) density dependence on T_g (for different T_c). Although the transition time from Tc to Tg was fixed to 20 seconds for all our experiments, there were some exceptions, in which T_c (900 °C) was significantly higher than T_g and a longer period was needed for cooling down to T_g below 700 °C. Those cases are denoted with a green x and the actual cooling time is noted next to the corresponding data points in (b) and (d).

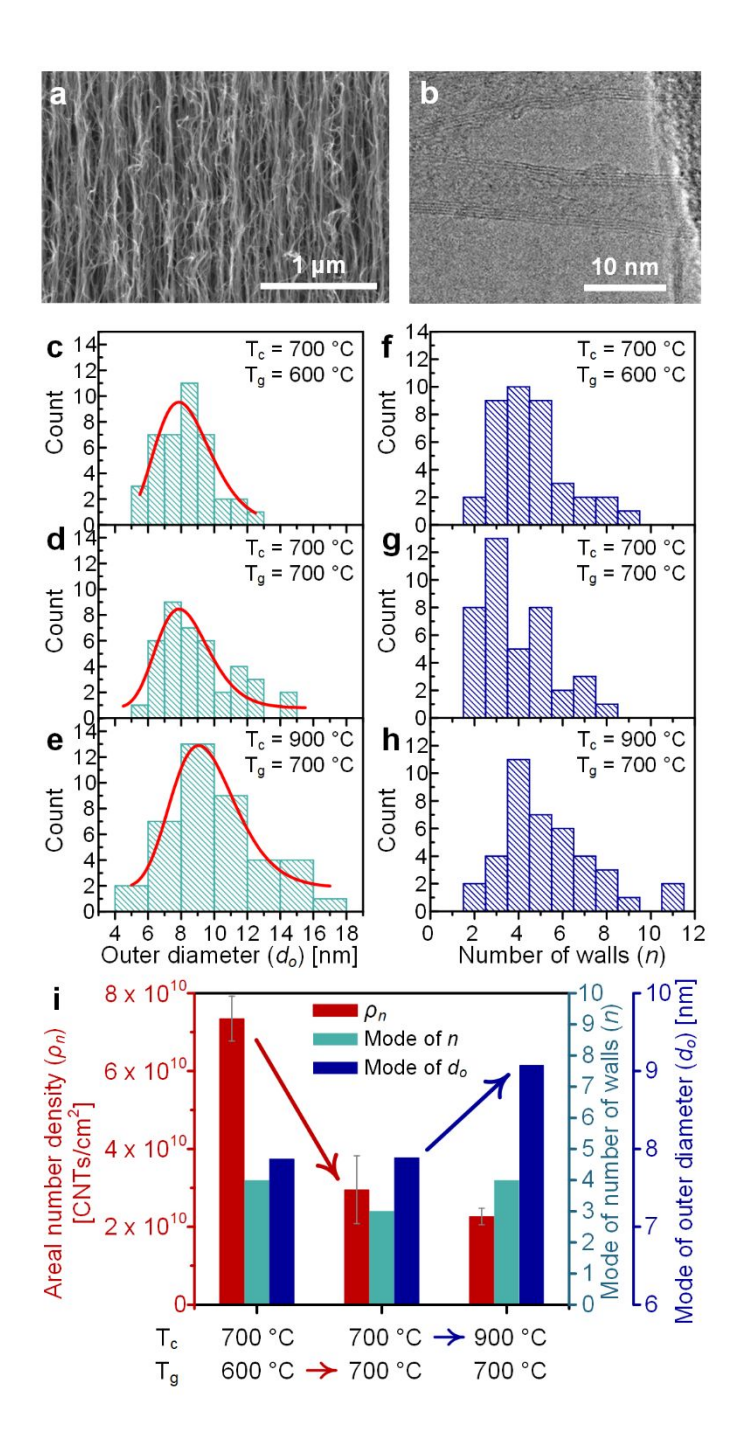


Fig. 4. Morphology and structure of CNTs. (a) An SEM image of CNTs grown at $T_p = 825$ °C, $T_c = T_g = 600$ °C. (b) A TEM image of a CNT grown at $T_p = 825$ °C, $T_c = 700$ °C, $T_g = 600$ °C. Distributions of (c – e) outer diameter and (f – h) number of walls of CNTs grown at $T_p = 825$ °C, $T_c = 700$ °C, $T_c = 700$ °C.

= 700 & 900 °C, T_g = 600 & 700 °C. (i) Results for areal number density of CNTs, mode of outer CNT diameter distribution and mode of CNT number-of-walls distribution fore forests grown at different T_c and T_g .

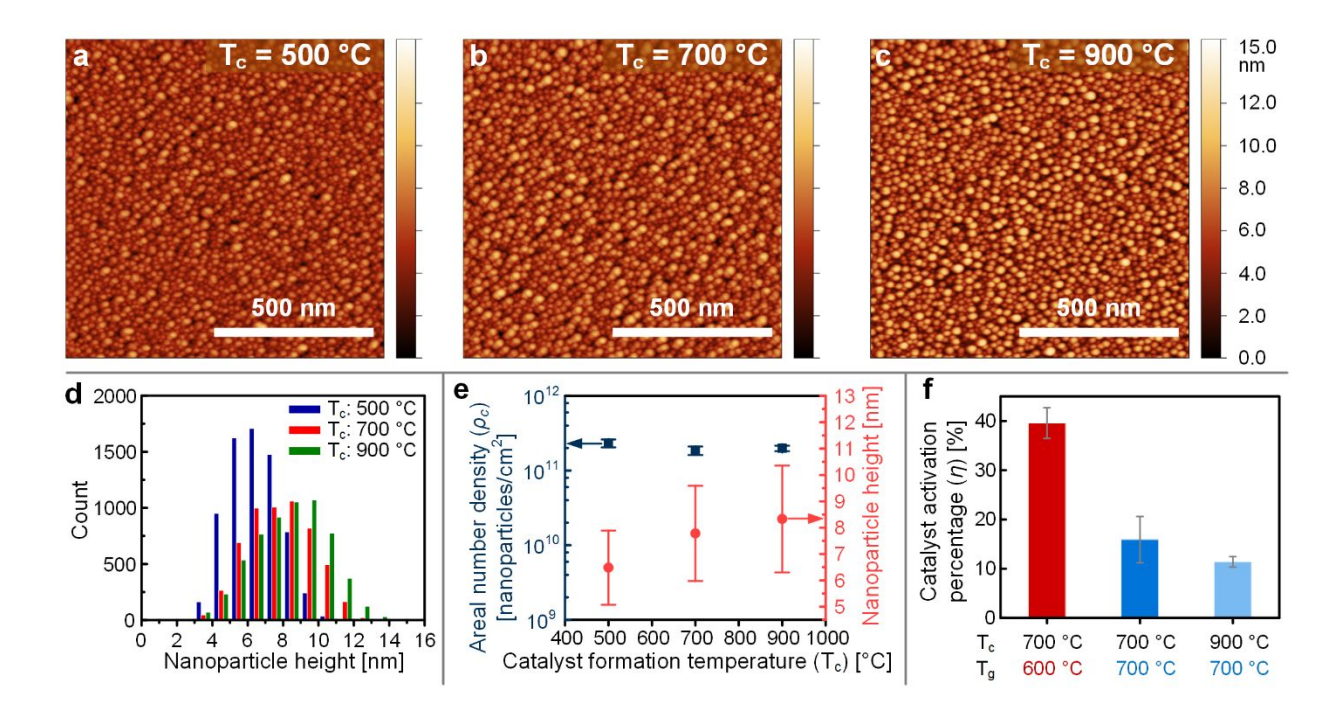


Fig. 5. (a – c) AFM images of catalyst nanoparticles formed at different T_c : (a) 500 °C, (b) 700 °C, and (c) 900 °C. (d) Histogram showing the distribution of height of nanoparticles formed at various T_c . (e) Areal number density and mean height of nanoparticles formed at various T_c . Error bars correspond to standard deviation. (f) Catalyst activation percentage at three sets of T_c and T_g . Data of nanoparticles in d-f was obtained from three AFM images for each T_c ; the rest of the AFM images are included in Fig. S4.

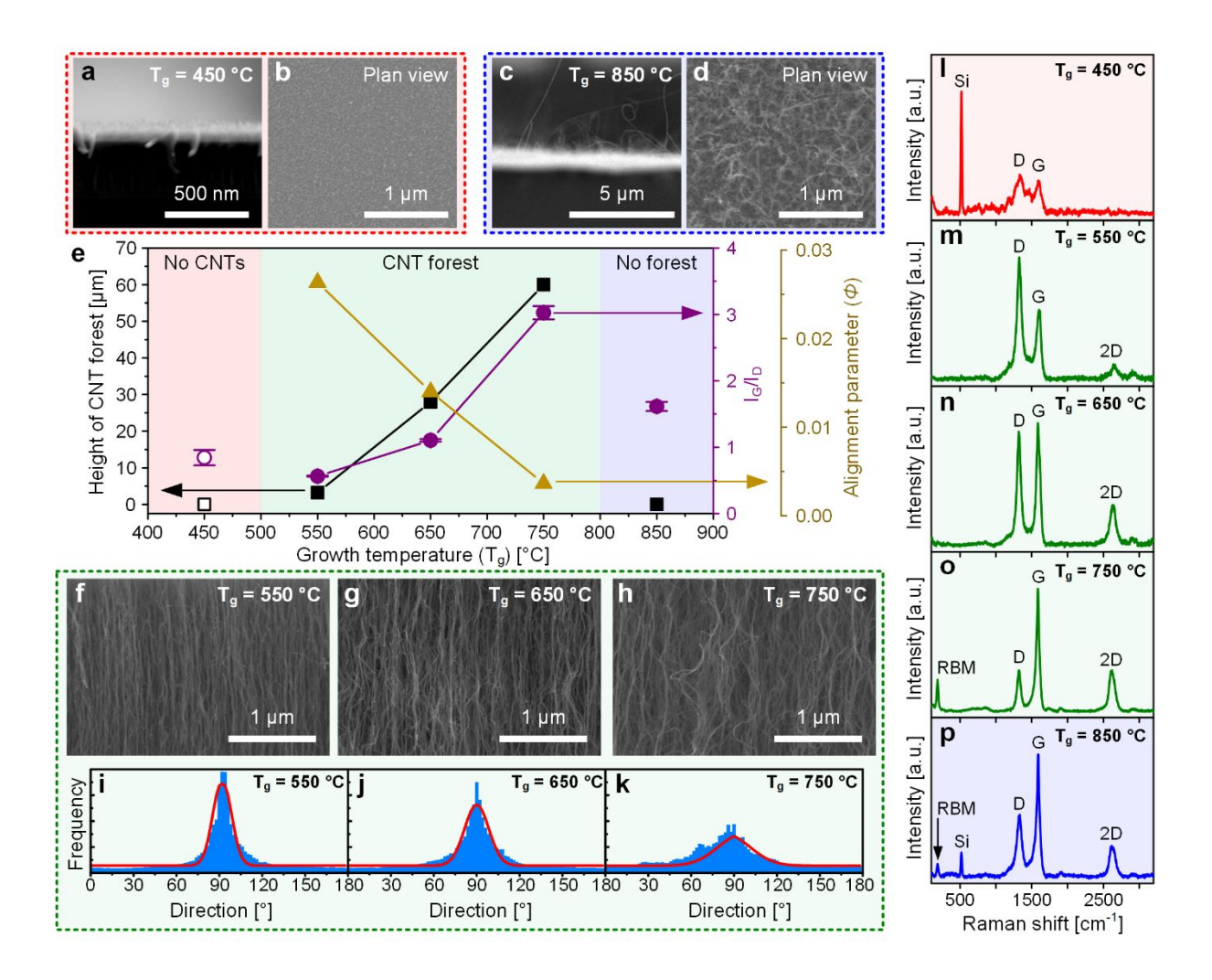


Fig. 6. Effect of T_g on the growth rate, alignment, and I_G/I_D ratio of the CNT forests grown for 2 min, while keeping T_p and T_c constant at 825 °C and 500 °C, respectively. SEM images at different T_g : (a) - (b) 450 °C and (c) - (d) 850 °C. (e) Plot of height, I_G/I_D ratio, and alignment parameter (Φ) of the CNT forests. SEM images of CNT forests grown at various T_g : (f) 550 °C, (g) 650 °C, and (h) 750 °C. Histogram resulting from Fourier component analysis of SEMs of CNT forests grown at various T_g : (i) 550 °C, (j) 650 °C, and (k) 750 °C. Raman spectra at various T_g : (l) 450 °C, (m) 550 °C, (n) 650 °C, (o) 750 °C, and (p) 850 °C.

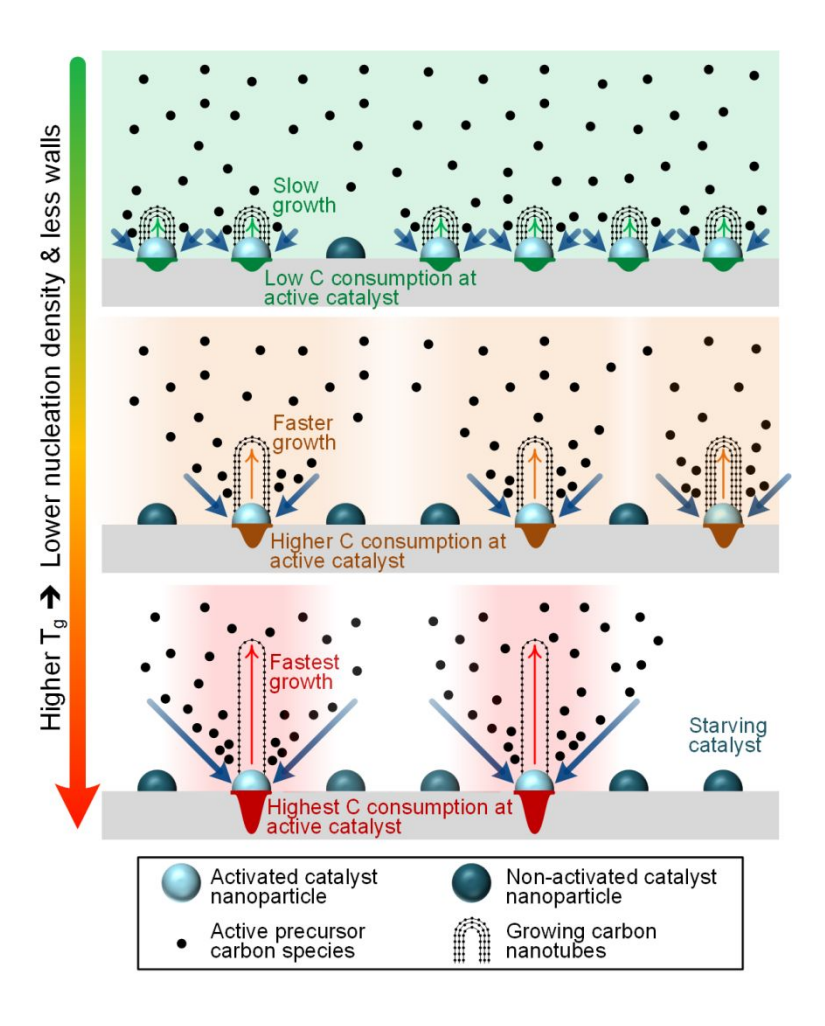


Fig. 7. Proposed mechanism of T_g -dependent CNT growth. Since T_p is constant, the supply rate of active precursor carbon species is the same regardless of T_g , but active carbon species are distributed differently at different T_g . At low T_g , the growth rates are generally slow, which leads to lower consumption rate of carbon at each active catalyst nanoparticle, and accordingly active carbon species are supplied evenly (indicated by the uniform green domain). At higher T_g , CNT growth rates become much faster, which leads to higher consumption rate of carbon at each active catalyst nanoparticle, and accordingly local depletion of active carbon species becomes dominant (indicated by the non-uniform orange and red domains/contours). This starvation of catalyst nanoparticles results in decreased number density of activated catalyst nanoparticles. At highest

 $T_{\rm g}$, the increased discrepancy between maximum carbon consumption rate and carbon supply rate at active catalyst nanoparticle also results in reduced number of walls and growth of SWCNTs instead of MWCNTs. In this figure, the plotted distribution of active carbon species represents an integral over growth time, and is not meant as an instantaneous concentration gradient. Moreover, the blue arrows are not meant to represent a specific directional flow, but rather are meant to indicate the local consumption of carbon at active catalyst nanoparticles at different rates depending on $T_{\rm g}$.

Table 1. Previous reports to decouple gas-phase reaction or catalyst formation from CNT growth.

Corresponding author	year	Main points	Gas-phase reaction	Catalyst	What enabled decoupling	Reference
Cheol Jin Lee	2001	Employed preheater to grow CNT forests at low substrate temperature	Decoupled	Coupled	Preheater	23
Young Hee Lee	e 2002	Employed tungsten wire filament to accelerate gas- phase decomposition Used Pd plate as a dual catalyst	Decoupled	Coupled	Tungsten wire filament	25
A. John Hart	2009	There are competing pathways between graphitic and amorphous carbon deposited during synthesis.	Decoupled	Coupled	Preheater	21
Carl V. Thompson	2009	Using preheater, low temperature growth was enabled.	Decoupled a)	Coupled	Preheater	24
Gilbert D. Nessim	2011	Precursor gas chemistry affects the crystallinity of CNTs	Decoupled	Coupled	Preheater	22
Hyung Gyu Park	2013	Thermal treatment of the acetylene precursor at 600-700 °C is found crucial for the synthesis of VA-CNTs.	Decoupled a)	Coupled	Temperature gradient within the reactor	26
Hyung Gyu Park	2018	Proposed a parallel reaction pathway model which takes gas-phase reaction into account.	Decoupled a)	Coupled	Temperature gradient within the reactor	27
Kenji Hata	2013	Catalyst formation and CNT growth process were decoupled Diameter and density are inversely correlated.	Coupled	Decoupled	Fast heating by infrared	28

Kenji Hata	2013	Larger diameter SWCNT would grow faster	Coupled	Decoupled	Fast heating by infrared	29
A John Hart	2016	More consistent growth is possible by stabilizing the moisture and hydrocarbon concentration between the catalyst formation step and the growth step.	Coupled	Decoupled b)	Moving the substrate	30
Mostafa Bedewy	2019	Present work	Decoupled	Decoupled	Preheater, and fast heating by infrared	

a) Temperature of gas-phase reaction zone affects the temperature of substrate. i.e., not perfectly decoupled.

b) The growth and catalyst formation were performed at the sample temperature, although the steps are decoupled.

TOC Graphic

